PCCP

PAPER

View Article Online
View Journal | View Issue

Cite this: *Phys. Chem. Chem. Phys.*, 2024, **26**, 8973

Opposing roles of organic salts on mini-protein structure†

Pei-Yin Lee,[a] Onkar Singh,[b] Neha Nanajkar,[c] Harry Bermudez *[b] and Silvina Matysiak *[d]

We investigated the effects of 1-ethyl-3-methylimidazolium chloride ([EMIM][Cl]) and choline chloride ([Chol][Cl]) on the local environment and conformational landscapes of Trp-cage and Trpzip4 mini-proteins using experimental and computational approaches. Fluorescence experiments and computational simulations revealed distinct behaviors of the mini-proteins in the presence of these organic salts. [EMIM][Cl] showed a strong interaction with Trp-cage, leading to fluorescence quenching and destabilization of its native structural interactions. Conversely, [Chol][Cl] had a negligible impact on Trp-cage fluorescence at low concentrations but increased it at high concentrations, indicating a stabilizing role. Computational simulations elucidated that [EMIM][Cl] disrupted the hydrophobic core packing and decreased proline-aromatic residue contacts in Trp-cage, resulting in a more exposed environment for Trp residues. In contrast, [Chol][Cl] subtly influenced the hydrophobic core packing, creating a hydrophobic environment near the tryptophan residues. Circular dichroism experiments revealed that [Chol][Cl] stabilized the secondary structure of both mini-proteins, although computational simulations did not show significant changes in secondary content at the explored concentrations. The simulations also demonstrated a more rugged free energy landscape for Trp-cage and Trpzip4 in [EMIM][Cl], suggesting destabilization of the tertiary structure for Trp-cage and secondary structure for Trpzip4. Similar fluorescence trends were observed for Trpzip4, with [EMIM][Cl] quenching fluorescence and exhibiting stronger interaction, while [Chol][Cl] increased the fluorescence at high concentrations. These findings highlight the interplay between [EMIM][Cl] and [Chol][Cl] with the mini-proteins and provide a detailed molecular-level understanding of how these organic salts impact the nearby surroundings and structural variations. Understanding such interactions is valuable for diverse applications, from biochemistry to materials science.

Received 17th November 2023,
Accepted 22nd February 2024

DOI: 10.1039/d3cp05607d

rsc.li/pccp

1 Introduction

The maintenance, or extension, of protein stability constitutes an important goal in biotechnology. Once a protein has lost its native structure it ceases to be useful. Over the last recent years many efforts have explored ionic liquids (ILs), a subclass of organic salts, to modulate protein stability.[1–5] Many of these studies focus on globular proteins such as lysozyme, ribonuclease A, lipases, hemoglobin, green fluorescent protein and cytochrome *c*, to name a few.[5–18] These studies typically concentrate on examining the impacts of ILs on particular tertiary structures or on specific long-range non-bonded interactions, thereby complicating the process of drawing conclusions about the influence of certain ILs on specific secondary structures. Therefore, it becomes desiring, and necessary to look at how certain type of organic salts interact with mini-proteins that contain unique secondary structures.[19,20] In this work we focus on the effect of organic salts in α-helical and β-sheet folds. For model systems we have chosen Trp-cage and Trpzip4. Trp-cage, a 20-residue mini-protein, has an α-helix and a 3_{10}-helix. It also has a hydrophobic core formed by aromatic residues and Pro residues. Trpzip4, a 16-residue peptide, is a β-hairpin itself. The β-hairpin is intact due to the strong hydrophobic interactions from four Trp residues. These two mini-proteins have been studied broadly as benchmark systems due to their representative secondary structure and their small size that allows for a robust sampling of their configuration space.[21–26]

Trp-cage, as a benchmark protein for the study of helix secondary structure, has been found both stabilized and destabilized through different organic salts.[27] In a circular dichroism experiment, the helical content of Trp-cage in neat [C_4mpy][Tf_2N] is enhanced through the N-terminal end with preferred intra-

[a] *Chemical Physics Program, Institute for Physical Science and Technology, University of Maryland, College Park, USA*
[b] *Department of Polymer Science and Engineering, University of Massachusetts, Amherst, MA, USA. E-mail: bermudez@umass.edu; Tel: +1 413 577 1413*
[c] *Department of Biology, University of Maryland, College Park, USA*
[d] *Fischell Department of Bioengineering, University of Maryland, College Park, USA. E-mail: matysiak@umd.edu; Tel: +1 301 405 0313*

† Electronic supplementary information (ESI) available. See DOI: https://doi.org/10.1039/d3cp05607d

peptide hydrogen bonding.[26] Whereas another set of replica exchange MD simulations found that [EMIM][Act] denatures Trp-cage in a cold denaturation fashion. In this case, the helix is mostly intact, while the whole tertiary structure is loosened.[28] Trpzip4, which is a modified variant of GB1 hairpin, often serves as a benchmark for stable β-hairpin. From experiment, neat [C_4mpy][Tf_2N] is observed to denature Trpzip4 through interactions between the alkyl groups of the IL and Trp residues that form the hydrophobic core.[26] Simulations have found that $[EMIM]^+$ based ILs with different anions can exert a different degree of denaturation on GB1 hairpin, with decreasing effect as the following order: acetate, $[BF_4]^-$, $[Cl]^-$.[29] In the case of [EMIM][Act], the anions are determined to be the driving force for denaturation, not the cations.[30] It occurs that, similar to large globular proteins, the stabilization or destabilization of these mini-proteins also depends on the combination of IL cation and anion, and more comprehensive studies combining both experiments and simulations are needed.

While wet lab experiments such as fluorescence spectroscopy and circular dichorism could provide a wealth of knowledge on the change of hydrophobic environment and secondary structure caused by organic salts and other co-solutes, microscopic insights are often lacking.[31–34] MD simulations are therefore used to complement these deficiencies. However, the viscous nature of organic salt solutions and ILs strongly limits the application of ordinary atomistic MD. Even though the peptides we focus here are small in size, convergence in sampling still requires long temporal scale, which is often not realistic. Here we apply a newly developed coarse-grained (CG) MD model named protein model with polarizability and transferability (*ProMPT*) to leverage sampling efficiency. CG models group similar functional groups into beads to reduce the degree of freedom and thus smoothen the free energy landscape, allowing fast sampling of folding events. The novelty of *ProMPT* is the implementation of charged dummy sites on the polar beads that can response to environment stimulus and result in change of dipole moment. The addition of structural polarization allows us to sample protein folding events. *ProMPT* has been applied successfully to both Trp-cage and Trpizip4 in reproducing the atomistic potential of mean force (PMF) and native structure.[35] The organic salts will also be modeled with the same philosophy of *ProMPT*.

We selected cations commonly found in organic salts, specifically choline and imidazolium, to examine their effects on the mini-proteins Trp-cage and Trpzip4. [Chol][Cl] emerges as a promising candidate for an organic salt due to the natural compound $[Chol]^+$, which exhibits high bio-compatibility and potential applications as a vaccine additive. Moreover, $[Chol]^+$-based organic salts have previously been reported as protein stabilizers, whereas $[EMIM]^+$-based ILs are often known as denaturants, providing a counterexample. In this study, we employ a combination of experiments and simulations to investigate how these two major organic cations modulate specific secondary structures.

2 Materials and methods

2.1 Simulation setup

All CG simulations are performed with GROMACS 2019.4.[36] Initial conformations for Trp-cage and Trpzip4 are unfolded/extended and generated with an in-house code. The amino acid sequences are taken from the protein data bank (1l2y.pdb for Trp-cage and 1le3.pdb for Trpzip4).[37–39] The *ProMPT* force field is employed to model the two mini-proteins.[35] The corresponding mapping scheme converting atomistic conformation to CG conformation for peptides is illustrated in Fig. 1. To simulate [EMIM][Cl], we employed the imidazolium-based ionic-liquid MARTINI force field, which is compatible with our mini-protein force field (*ProMPT*).[35,40] For [Chol][Cl], we adopted the MARTINI parameterization scheme for imidazolium-based ionic liquids.[40] Validations for [Chol][Cl] can be found in the ESI.† The CG mapping scheme for both $[Chol]^+$ and $[EMIM]^+$ is shown in Fig. 2, where the mapping scheme for $[EMIM]^+$ is inspired from MARTINI3[41] and modified to be used with *ProMPT*. For $[Chol]^+$, the bead type for the positively charged one bead is TQ0, and the bead type for the polar bead is PNa (taken from *ProMPT*). The PNa bead also carries two dummies (bead type: D2) with partial charges ±0.32. The bond length between TQ0 and PNa bead is 0.47 nm with a force constant of 1250 kJ mol^{-1} nm^{-2}. $[EMIM]^+$ is constituted by three sub-size hydrophobic beads as a ring structure (SC6, TC6h, and TC5h), with SC6 and TC6h bead each carrying a positive 0.5 partial charges. The constraint between SC6 and TC6h/TC5h is 0.285 nm, while between TC6h and TC5h is 0.315 nm. CG bead type TQa is parametrized for chloride anion. The Lennard-Jones potential parameters, such as the depth of the well (ε) and the distance where the potential is zero (σ), for the two ILs are provided in Table S1 (ESI†). Additional information about other bead types can be found in the original paper of *ProMPT*.[35]

Three solvent systems are studied with each peptide: water, 25 wt% [Chol][Cl], and 25 wt% [EMIM][Cl]. The number of water, organic salt molecules, and counterion CG molecules are listed in Table 1. The Yesylevsky *et al.*'s polarizable water model is used to model water molecules, which also has a 1 to 4 mapping.[42] Energy minimization with steepest decent method is first performed and followed by a short NPT equilibration (50000 steps with each step as 1 fs) at 350 K. Production runs at

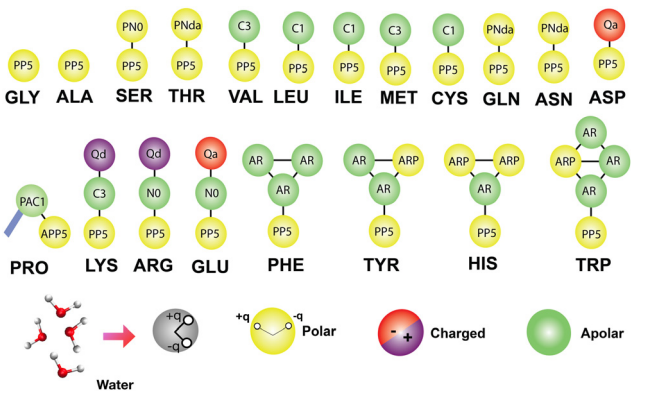

Fig. 1 *ProMPT* CG mapping scheme, where the polar bead is shown in yellow, charged bead is shown in red/purple, and hydrophobic bead is shown in green. The bead type is also labeled on each bead. The Yesylevsky *et al.*'s polarizable water model is used to model water molecules and has a 1 to 4 mapping.[42]

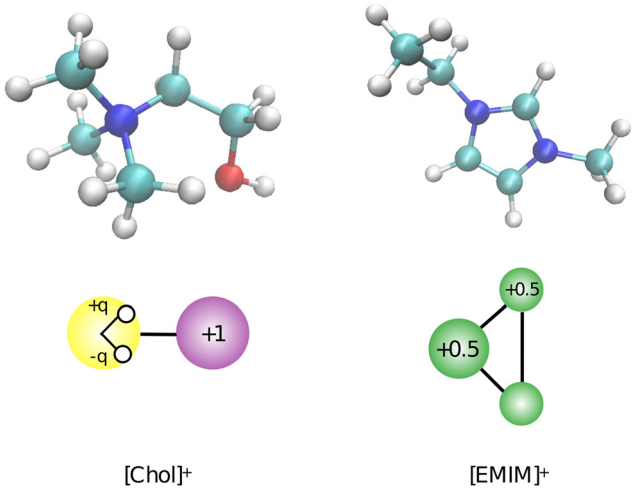

Fig. 2 CG mapping scheme for $[Chol]^+$ and $[EMIM]^+$. The upper figures are atomistic conformations, where cyan: carbon, blue: nitrogen, red: oxygen, and white: hydrogen. The lower figures are the corresponding CG conformations, where the positive bead is in purple, polar bead is in yellow, and hydrophobic beads are in green. For the CG $[EMIM]^+$, the two beads carrying 0.5 partial charges are also labeled.

15 different temperatures (from 350 K to 700 K, every 25 K) with NVT ensemble are then performed for 500 ns with a time step of 10 fs. Particle-mesh Ewald (PME) method is applied for long range electrostatic interactions[43] with a cutoff of 1.6 nm. Nosé–Hoover thermostat is used to maintain the system at the desired temperature[44] and the LINCS algorithm was used to evaluate constraints.[45]

2.2 Analyses

Free energy profiles are constructed for both Trp-cage and Trpzip4 using backbone (BB) native contact fraction and root-mean-squared-deviation (RMSD) as two reaction coordinates. The backbone native contact fraction computes the distance matrix between each backbone bead of the peptide and considers only the pairs that are within a cutoff (6.5 Å for Trp-cage and 7 Å for Trpzip4) and exist in the native PDB-converted-CG conformation. For Trp-cage, RMSD only considers the α-helix region (residue 1 to 9), while for Trpzip4 the whole peptide is considered. Multistate Bennett Acceptance Ratio (MBAR) method takes the last 420 ns data from each simulated temperature and it is used to generate the free energy profiles and the distribution of the number of cation-aminoacid and Pro-aromatic contacts at the lowest simulated temperature (350 K) from the 15 temperature runs.[46] The cutoff used to compute the number of cation-aminoacid and Pro-aromatic contacts is 4 Å and 6 Å, respectively. All the insert images are rendered from VMD.[47]

Table 1 Number of CG molecules in each system

	System	Water	$[Chol]^+$ or $[EMIM]^+$	$[Cl]^-$	Counterions
Trp-cage	water	1957	0	0	1 Cl^{-1}
	25 wt% [Chol][Cl]	1400	252	252	1 Cl^{-1}
	25 wt% [EMIM][Cl]	1399	229	229	1 Cl^{-1}
Trpzip4	water	1610	0	0	3 Na^{+1}
	25 wt% [Chol][Cl]	1400	252	252	3 Na^{+1}
	25 wt% [EMIM][Cl]	1397	229	229	3 Na^{+1}

2.3 Materials

The two peptides (>98%) were purchased from Genscript. Trp-cage is 20 amino acids in length and its single-letter sequence is NLYIQWLKDGGPSSGRPPPS. Trpzip4 is 16 amino acids in length and its single-letter sequence is GEWTWDDATKTWTWTE. Potassium phosphate monobasic (>99%), potassium phosphate dibasic (99.5%), and [Chol][Cl] (99%) were purchased from Fisher Scientific. [EMIM][Cl] (>95%) was purchased from Sigma-Aldrich. Unless otherwise indicated all materials were used without further purification.

2.4 Fluorescence spectroscopy

A photoluminescence spectrometer from Photon Technology International was used for the fluorescence measurements. The peptides were used at a concentration of 1 mg mL^{-1}. The intrinsic tryptophan fluorescence was monitored with an excitation wavelength of 280 nm in quartz cuvette having a path length of 10 mm. The emission spectra were recorded between 285 to 485 nm keeping the excitation and emission slit widths at 0.5 mm. All above experiments were performed at room temperature.

Possible contributions due the inner filter effect (IFE)[48,49] were considered. The 'primary' IFE is known to be both sample- and instrumentation-dependent. However, our fluorescence data are all performed with the same concentration of peptide and the same concentration range of quencher. Therefore the correction factor for the primary IFE would be constant across all samples. The 'secondary' IFE is especially relevant to quenching experiments like those performed here. Fortunately [EMIM][Cl] does not absorb at the excitation wavelength used (*i.e.*, 280 nm). This quencher only absorbs below the far-UV range (*i.e.*, below 225 nm),[50] and therefore the secondary inner filter effect is not present.

2.5 Circular dichroism

The CD spectra were recorded in the far-UV region (190–260 nm) on a Jasco J-1500 spectrophotometer at 20 ± 1 °C, with a quartz cuvette having path length of 1 mm. The peptides were used at a concentration of 1 mg mL^{-1}. The data pitch was set to 1 nm and bandwidth was set to 1 nm, with a scanning speed of 100 nm min^{-1}.

3 Results

3.1 Fluorescence shows contrasting roles for each IL

As their names suggest, Trp-cage and Trpzip4 contain tryptophan residues, one and four, respectively. The intrinsic fluorescence of these tryptophan residues was monitored with the addition of [Chol][Cl] and [EMIM][Cl], to gain insight into changes of the local environment. For Trp-cage, the effects of [EMIM][Cl] and [Chol][Cl] are dramatically different. Addition of [EMIM][Cl] at less than 1 wt% (millimolar concentration)

quenches Trp-cage fluorescence. From this quenching a binding constant can be calculated *via* the Benesi–Hildebrand equation $1/(F - F_0) = 1/(F_{max} - F_0) + 1/(F_{max} - F_0)KC$, where F_0, F, F_{max} are the fluorescence intensities in the absence, intermediate, and excess concentration of the additive at a concentration C.[51,52] Fig. 3 shows the expected linear relationships, but as pointed out by others, double-reciprocal plots can nevertheless be subject to errors.[53] Therefore, we also analyzed the fluorescence data using nonlinear regression (Fig. S2, ESI†).[54] We obtained similar binding constants irrespective of the analysis method, and here we report the values from nonlinear regression.

The binding constant for [EMIM][Cl] to Trp-cage is calculated as $K \approx 5.4\ M^{-1}$. Even a weak interaction would be expected to destabilize the native structural interactions within the peptide. By contrast, addition of [Chol][Cl] at 1 wt% has a negligible effect on Trp-cage fluorescence. At concentrations exceeding 12 wt% [Chol][Cl], Trp-cage fluorescence actually increases. This suggests a stabilizing role, if any, for [Chol][Cl] on Trp-cage. Moreover the maximum emission wavelength λ_{max} of Trp-cage changes in opposite directions for [EMIM][Cl] and [Chol][Cl]. In the case of [Chol][Cl], λ_{max} is blue-shifted, whereas in the case of [EMIM][Cl], λ_{max} is red-shifted (as shown in Fig. S3 and S4, ESI†). These shifts are consistent with more hydrophilic/exposed and hydrophobic/buried environments, respectively.[55]

For Trpzip4, very similar results to Trp-cage were seen *via* fluorescence, with [EMIM][Cl] quenching fluorescence and the corresponding binding constant being much larger than that for Trp-cage, with $K \approx 30\ M^{-1}$. Interestingly, Trpzip4 has 4 times as many tryptophan residues as Trpcage, and its binding constant with [EMIM][Cl] is roughly 5 times larger. This suggests a significant role for π–π and cation–π interactions between the peptide aromatic and the quencher imidazolium groups,[56] reminiscent of a previous study by our group with lysozyme and a related IL.[57] Like for Trpcage, the addition of [Chol][Cl] also increased Trpzip4 fluorescence, but again only at high concentrations. The maximum emission wavelength λ_{max} of Trpzip4 also followed the same pattern as Trp-cage. Overall, the fluorescence results suggest similar roles of these ILs on both peptides (and their secondary structures).

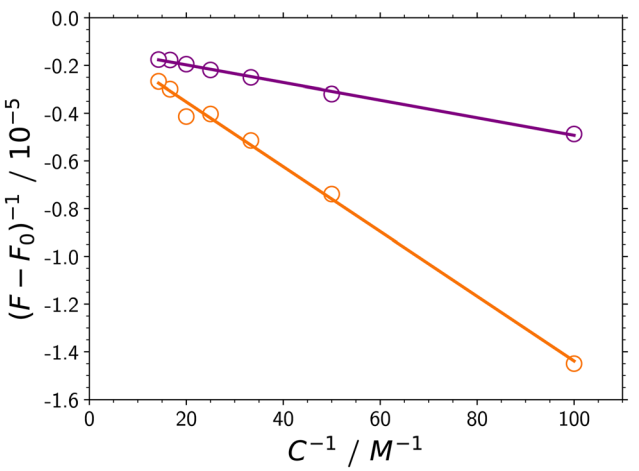

Fig. 3 Benesi–Hildebrand plots from tryptophan fluorescence quenching of Trpcage (orange) and Trpzip4 (purple) with added [EMIM][Cl].

3.2 Circular dichroism shows stabilization by [Chol][Cl]

The secondary structures of Trp-cage and Trpzip4 were experimentally probed using far-UV circular dichroism (CD). Unfortunately, the imidazolium cation $[EMIM]^+$ exhibits very strong absorbance in this wavelength region, precluding CD studies for [EMIM][Cl].[58] Nevertheless the effect of [Chol][Cl] on both peptides could be studied.

The CD spectra of Trp-cage (Fig. 4(a)) shows that the effect of [Chol][Cl] is to stabilize its secondary structure (a mixture of α-helix and 3_{10}-helix). The increasing signal with added [Chol][Cl] is opposite to the trend observed in thermal denaturation of Trp-cage,[59] and in urea denaturation of α-helical alanine-rich peptides[60] To calculate the extent of secondary structure stabilization caused by [Chol][Cl], the ellipticity at 222 nm θ_{222} is used to obtain the fraction of α-helical content f.[61] The initial helix fraction f_0 is calculated from the known structure (PDB: 1L2Y) as $f_0 = 0.45$, and because f is proportional to θ_{222}, it can be seen that the α-helical fraction slowly increases reaching a plateau value of $f \approx 0.60$ at 33 wt% [Chol][Cl].

Another measure of Trp-cage structure is the peak ratio $R = \theta_{222}/\theta_{208}$ (Fig. 4(a), inset). This ratio has been used to characterize 3_{10} helices,[62,63] where $R \approx 0.4$, which contrasts with "pure" α-helices where $R \approx 1.0$.[64] Because Trp-cage has contributions from both α-and 3_{10} helices, it is not surprising that we find $R = 0.62$ in the absence of [Chol][Cl] (in between the two extremes). With added [Chol][Cl] this ratio increases linearly up to a maximum of $R = 0.71$, indicating a progressive shift towards greater α-helical content in Trp-cage.

Similar to the case of [Chol][Cl] on Trp-cage, we also see a stabilizing effect of [Chol][Cl] on Trpzip4 (Fig. 4(b)), with the increasing CD signal trending opposite to that of thermal denaturation.[24] A deeper level of insight here is precluded because the analytical treatment of β-turns is less well-developed than for α-helices. Nevertheless, because the helices and turns of Trp-cage and Trpzip4 are both mediated by intrapeptide hydrogen bonding, it therefore appears that [Chol][Cl] (at high concentrations) strengthens these interactions.

3.3 Molecular simulations offers a molecular view of the conformational changes in Trp-cage and Trpzip4

The conformational landscapes of Trp-cage and Trpzip4 were characterized through coarse-grained molecular dynamics simulations. In water (Fig. 5(a)) and 25 wt% [Chol][Cl] (Fig. 5(b)), Trp-cage exhibited highly similar free energy landscape plots, featuring a folded basin located at an RMSD helix BB range of 0.08 to 0.13 nm and a native contact fraction of 0.65 to 0.8. Although the folded states (blue) were slightly more populated in water compared to 25 wt% [Chol][Cl], the difference was not significant. However, in the free energy landscape of 25 wt% [EMIM][Cl] (Fig. 5(c)), a more rugged landscape was observed compared to water and 25 wt% [Chol][Cl]. The folded basin

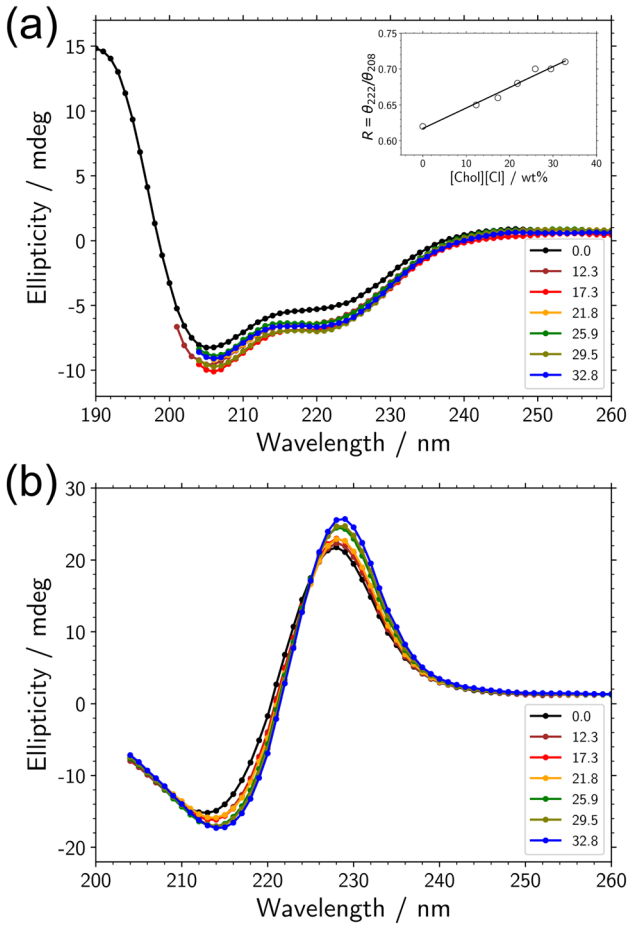

Fig. 4 Circular dichroism spectra with increasing [Chol][Cl] (concentrations in wt%) for (a) Trp-cage and (b) Trpzip4. The inset to (a) is the ratio $R = \theta_{222}/\theta_{208}$.

shifted to an RMSD helix BB range of 0.08 to 0.15 nm, with a native contact fraction ranging from 0.57 to 0.62. The RMSD helix BB remained the same for all three systems, but a shift towards lower native contacts was observed for [EMIM][Cl]. The reduction in native contacts indicated a disruption of the tertiary structure, despite the helix remaining intact. Additionally, a clear unfolded basin was observed at an RMSD helix BB range of 0.2 to 0.35 nm, with a native contact fraction ranging from 0.38 to 0.40. The observed changes on the free energy landscape of 25 wt% [EMIM][Cl] compared to water and 25 wt%[Chol][Cl] suggest a destabilizing role of [EMIM][Cl] on tertiary structure of Trp-cage. Computationally, the helicity in Trp-cage was unaffected by both ionic liquids. Although the secondary structural content could not be assessed experimentally with [EMIM][Cl], the fact that [Chol][Cl] did not destabilize the helicity in Trp-cage aligns with the stabilization observed from the CD data. This disruption of the tertiary structure, but not the secondary structure, induced by $[EMIM]^+$ has been previously reported with the same protein in [EMIM][Act], which resembles cold unfolding.[28]

We continue our investigation into the destabilizing effect of [EMIM][Cl] on Trp-cage from a molecular perspective. Fig. 6(a) displays the distribution number of contacts between the cation ($[EMIM]^+$ or $[Chol]^+$) and amino acids of Trp-cage. The plot distinctly indicates that $[Chol]^+$ lacks specific interactions with the mini-protein compared to $[EMIM]^+$. A notable preference for interactions between $[EMIM]^+$ and the aromatic groups, aspartate (Asp), and prolines (Pro) is evident. Although $[Chol]^+$ does exhibit interactions with Asp and the aromatic amino acids, they are less pronounced in comparison. The heightened hydrophobicity of $[EMIM]^+$ compared to $[Chol]^+$, may account for the observed disparities in contacts with aromatic groups. The fluorescence experiments further support the stronger binding of $[EMIM]^+$ to the aromatic groups than $[Chol]^+$, as they revealed a binding constant of $K \approx 6\ M^{-1}$ for [EMIM][Cl].

In Fig. 6(b), a representative structure of Trp-cage in water is shown, where the aromatic residues pack against the Pro residues at the C-terminal of the protein, forming a hydrophobic core. However, this hydrophobic core packing is slightly distorted in 25 wt %[Chol][Cl], as there is a loss of aromatic group-Pro residue contacts, as depicted in Fig. 7. The interactions between Pro residues and the aromatic groups can occur favorably through both the hydrophobic effect and the interaction between the π aromatic face and the polarized C–H

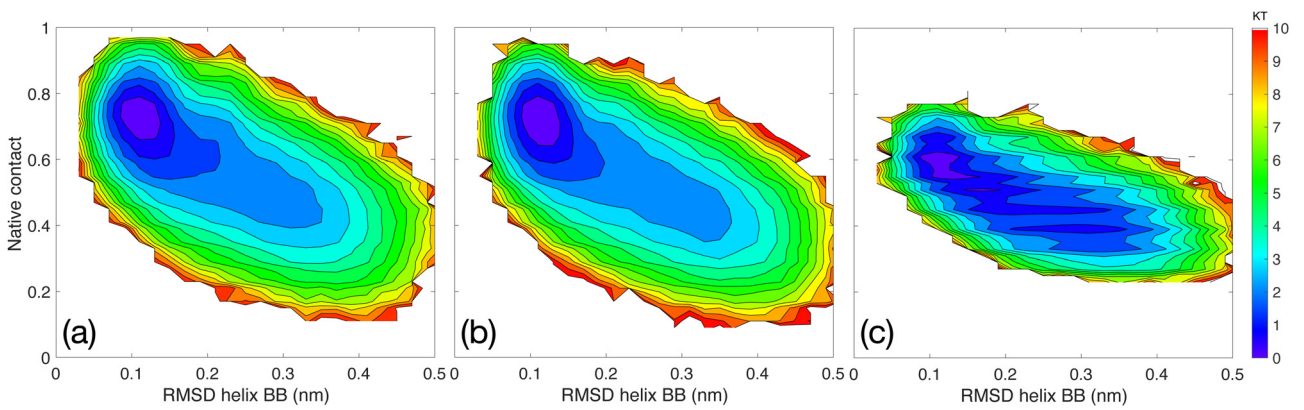

Fig. 5 Free energy landscape for Trp-cage at 350 K in (a) water, (b) 25 wt% [Chol][Cl], and (c) 25 wt% [EMIM][Cl]. *X*-Axis is the RMSD helix BB and *y*-axis is the native contact fraction. The energy scale is shown on the right with unit KT.

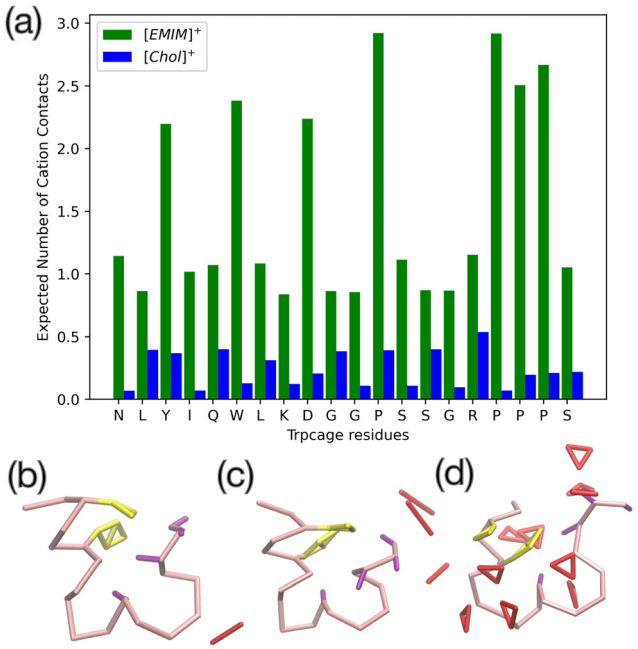

Fig. 6 (a) Distribution of the number of contacts between $[Chol]^+$ (blue) or $[EMIM]^+$ (green) and the different amino acids of Trp-cage within the folded basin at 350 K. Representative structure of Trp-cage within the folded basin at 350 K in (b) water; (c) 25 wt% [Chol][Cl] and (d) 25 wt% [EMIM][Cl]. Tyr and Trp residues are shown in yellow, Pro residues are shown in purple, while cations are shown in red.

bonds, known as the CH–π interaction. On the other hand, interactions between $[EMIM]^+$ and the two aromatic residues lead to a significant reorientation of these residues towards the solvent, as shown in Fig. 6(d).

The cation–π, π–π, and hydrophobic interactions between $[EMIM]^+$ and the aromatic groups, along with the CH–π interactions between Pro and $[EMIM]^+$, play a dominant role. These interactions overshadow the hydrophobic interactions that typically stabilize the core between Pro residues and the aromatic groups.

As a result, there is a decrease in the number of Pro-aromatic residue interactions, as shown in Fig. 7. The decrease of the

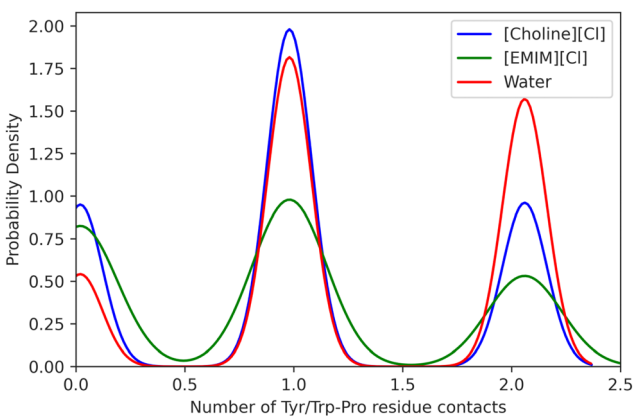

Fig. 7 Distribution of the number of aromatic residues near the Pro residues at the tail of Trp-cage within the folded basin at 350 K.

number of contacts between the cations and the Pro residues is predominant in the 25 wt% [EMIM][Cl] system. In this case, $[EMIM]^+$ enters the protein core, as depicted in Fig. 6(d), while $[Chol]^+$ does not penetrate it. Neither IL system causes deformation in the α-helix at the N-terminal. This finding aligns with previous observations for Trp-cage in [EMIM][Act].[28] The exposure of solvent-exposed aromatic residues in [EMIM][Cl] and the penetration of $[EMIM]^+$ inside the protein core explain the red-shift observed in the maximum emission wavelength of the fluorescence experiment. Conversely, in [Chol][Cl], the aromatic groups face the interior of the Trp-cage core, which explains the blue-shift in the maximum emission wavelength. The fact that $[Chol]^+$ does not penetrate the Trp-cage core may be attributed to the absence of π–π and CH–π interactions. However, a subtle shift in the packing of the hydrophobic core is observed in 25 wt% [Chol][Cl] compared to that in water. The interaction of $[EMIM]^+$ with aromatic residues has also been observed in our previous publication, where the same cation disrupts an Arg–Trp–Arg sandwich interaction that stabilizes lysozyme, leading to destabilization of the overall structure.[57]

Fig. 8 illustrates the free energy landscape for Trpzip4 in water and ILs. Similar to the findings for Trp-cage, the free energy landscape of Trpzip4 becomes more rugged in 25 wt% [EMIM][Cl], accompanied by a shift and reduction in the folded basin. In contrast, there is no significant difference observed in the free energy landscape between water and 25 wt% [Chol][Cl]. The folded basin for Trpzip4 in both water and [Chol][Cl] is located at RMSD BB 0.28 to 0.35 nm with a native contact fraction of 0.68 to 0.82. However, for the [EMIM][Cl] system, the folded basin shifts and diminishes, resulting in a lower native contact fraction (0.70 to 0.77). Additionally, a misfolded basin emerges at RMSD BB 0.25 to 0.38 with a native contact fraction of 0.43 to 0.47. The shrinking of the folded basin in 25 wt% [EMIM][Cl] and the increased ruggedness of the free energy landscape indicate that the β-hairpin structure of Trpzip4 is less stable compared to water and 25 wt% [Chol][Cl]. Conversely, since Trpzip4 exhibits a similar free energy landscape in water and 25 wt% [Chol][Cl], its secondary structure remains intact, as confirmed by CD experiments.

The analysis of cation-amino acid contacts (Fig. 9(a)) clearly demonstrates preferential binding of $[EMIM]^+$ to Trp and negatively charged amino acids such as Glu and Asp. In Trpzip4, while $[Chol]^+$ does show interactions with Trp and anionic amino acids, they are less pronounced compared to those observed with $[EMIM]^+$. This observation is consistent with the experimental fluorescence data, which indicates that in solutions containing [EMIM][Cl], the maximum emission wavelength is red-shifted, suggesting increased solvent exposure of the Trp residues.

Furthermore, upon comparing Fig. 6(a) and 9(a), it is evident that more contacts are formed between $[EMIM]^+$ in Trpzip4 than in Trp-cage, which is in good agreement with the fluorescence data presented in Fig. 3. These results support the notion of stronger binding of $[EMIM]^+$ with Trpzip4 compared to Trp-cage.

Fig. 9(b) and (c) showcase representative conformations of Trpzip4 in 25 wt% [Chol][Cl] and 25 wt% [EMIM][Cl],

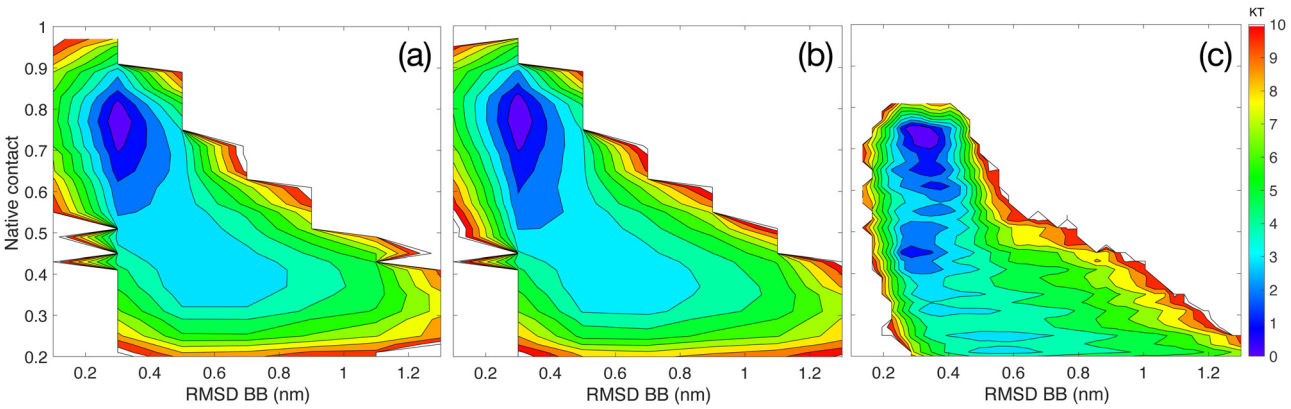

Fig. 8 Free energy landscape plots for Trpzip4 at 350 K in (a) water, (b) 25 wt% [Chol][Cl], and (c) 25 wt% [EMIM][Cl]. *X*-Axis is the RMSD BB and y-axis is the native contact fraction. The energy scale is shown on the right with unit KT.

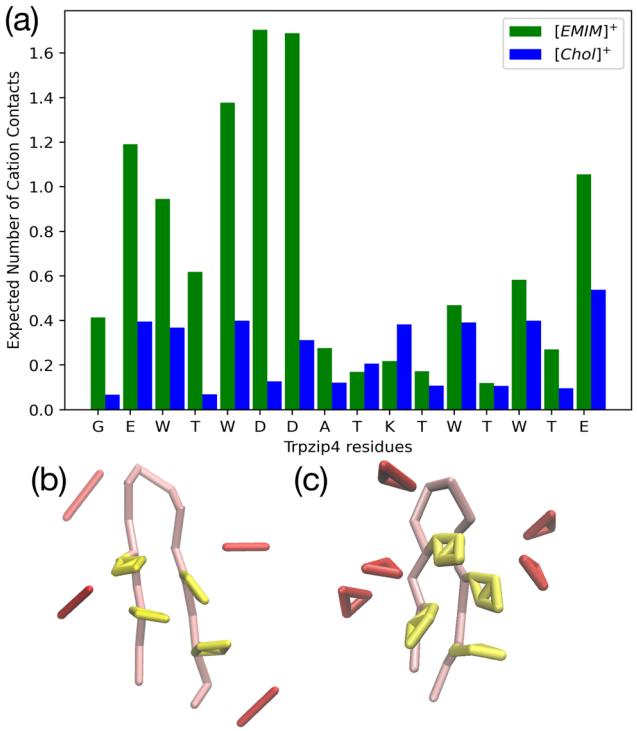

Fig. 9 (a) Distribution of the number of contacts between $[Chol]^+$ (blue) or $[EMIM]^+$ (green) and the different amino acids of Trpzip4 within the folded basin at 350 K. (b) A representative structure of Trpzip4 within the folded basin interacting with $[Chol]^+$ at 350 K. (c) A representative structure of Trpzip4 taken from the folded basin interacting with $[EMIM]^+$ at 350 K. Trp residues are shown in yellow and cations are shown in red.

respectively. The four Trp residues form the hydrophobic core for all cases, but the number of Trp–Trp contacts decreases dramatically for 25 wt% [EMIM][Cl] when compared to water and 25 wt% [Chol][Cl], as shown in Fig. S5 (ESI†).

In this context, $[EMIM]^+$ cations compete with the Trp–Trp hydrophobic interaction, and also with the Asp–Lys salt-bridge thereby reducing the stability of the β-hairpin. The cation–π and π–π interactions between $[EMIM]^+$ cations and the aromatic residues are also observed in Trp-cage and in our previous study on lysozyme.[57] These findings suggest a general rule that strong attractions between imidazolium-based cations and aromatic residues can serve as critical indicators for protein destabilization in ILs. In addition, disruption of salt-bridges can contribute significantly to lower β-hairpin stability.[65]

4 Discussion

The combination of experimental and computational findings sheds light on the effects of [EMIM][Cl] and [Chol][Cl] on the local environment and conformational landscapes of Trp-cage and Trpzip4 peptides. Computational and fluorescence experiments revealed distinct behaviors of Trp-cage and Trpzip4 in the presence of [EMIM][Cl] and [Chol][Cl]. [EMIM][Cl] quenched Trp-cage fluorescence, indicating a strong interaction and a destabilizing effect on the mini-protein's native structural interactions. Conversely, [Chol][Cl] had a negligible impact on Trp-cage fluorescence at low concentrations, but increased it at high concentrations, suggesting a stabilizing role. The observed red-shift in the maximum emission wavelength for [EMIM][Cl] and blue-shift for [Chol][Cl] corresponded to more hydrophilic/exposed and hydrophobic/buried environments, respectively. In Trp-cage, the simulations show that [EMIM][Cl] has higher binding with aromatic, anionic and Pro residues when compared to [Chol][Cl]. The enhanced binding of the aromatic and Pro residues by $[EMIM]^+$ disrupts the hydrophobic core packing and leads to decreased Pro-aromatic residue contacts which creates a more exposed environment to the Trp residues. Conversely, [Chol][Cl] subtly influences the hydrophobic core packing which goes in line with an hydrophobic environment near the Trp residues. The simulations also demonstrate a more rugged free energy landscape for Trp-cage in [EMIM][Cl], indicating a destabilizing effect on the tertiary structure.

Trpzip4 exhibited similar fluorescence trends to Trp-cage, with [EMIM][Cl] quenching fluorescence and a larger binding constant indicating a stronger interaction. The stabilizing effect of [Chol][Cl] on Trpzip4 fluorescence was also observed at high concentrations. The maximum emission wavelength changes

followed the same pattern as Trp-cage, supporting the role of [EMIM][Cl] in exposing solvent-exposed aromatic residues and [Chol][Cl] in burying them. The simulations for Trpzip4 demonstrate the preferential binding of [EMIM][Cl] to Trp residues in addition to binding to anionic amino acid. The computational observation of $[EMIM]^+$ exhibiting stronger binding to aromatic groups compared to $[Chol]^+$ aligns with fluorescence experiments, which revealed binding constants of $K \approx 5.4 M^{-1}$ for Trp-cage and $K \approx 30 M^{-1}$ for Trpzip4. Additionally, the computational finding of $[EMIM]^+$ penetrating the Trp-cage core is consistent with the experimental observation of a red-shifted maximum emission wavelength, suggesting increased solvent exposure for Trp amino acids. As observed in Trp-cage, the binding of $[Chol]^+$ to these amino acids is greatly reduced. These differences in binding might be explained by the heightened hydrophobicity of $[EMIM]^+$ compared to $[Chol]^+$. The free energy landscape analysis suggests a less stable β-hairpin structure in [EMIM][Cl].

Circular dichroism (CD) experiments provided valuable insights into the secondary structure of Trp-cage and Trpzip4 peptides. Our findings revealed that the presence of [Chol][Cl] led to the stabilization of the secondary structure in both peptides. Interestingly, at the computationally explored concentrations, we did not observe any significant changes in the secondary content of these peptides.

The differences observed in how the cations modulate the mini-protein conformational landscape are likely attributed to their distinct interactions with the mini-proteins. Specifically, $[EMIM]^+$ exhibited a stronger interaction with these mini-proteins, whereas $[Chol]^+$ showed minimal interaction at the folded basin. We speculate that the enhanced secondary structure observed in the presence of substantial $[Chol]^+$ may be attributed to indirect effects, such as changes in the dielectric environment. In simulations, we observe a 21% reduction in the dielectric constant compared to pure water when the concentration of [EMIM][Cl] is 25 wt%, and a 63% reduction for 25 wt% [Chol][Cl]. Previous computational evidence has demonstrated that a decreased dielectric constant enhances helical propensity. This reduction in the dielectric constant can lead to desolvation of the backbone CO and NH groups, resulting in stronger and more aligned hydrogen bonds between four consecutive residues.[66] A similar effect might be in place for the hydrogen bonds of a β-hairpin such as Trpzip4. From our simulations, we did not observe the stabilizing effects of $[Chol]^+$ compared to water on the secondary structural content of Trpzip4 and Trp-cage peptides at the studied concentrations. The secondary structure remained unchanged in the presence of $[Chol]^+$, which contrasts with the experimental findings. We hypothesize that these discrepancies between experiments and simulations may arise from the simplified nature of the coarse-grained model, which might not accurately capture the change in backbone dipole with changes of the dielectric medium.

5 Conclusion

In conclusion, the experimental and computational investigation conducted provides insight into the impact of [EMIM][Cl] and [Chol][Cl] on the local environment and conformational landscapes of Trp-cage and Trpzip4 peptides. Fluorescence experiments indicate distinct behaviors, with [EMIM][Cl] quenching Trp-cage fluorescence, suggesting destabilization, while [Chol][Cl] shows a stabilizing effect. Computational simulations reveal specific interactions between the mini-proteins and cations, with [EMIM][Cl] disrupting hydrophobic core packing and [Chol][Cl] subtly influencing it. Circular dichroism experiments demonstrate secondary structure stabilization in both mini-proteins with [Chol][Cl].

Data availability

All files required to set up and perform the simulations described in this work can be found at: **https://www.matysiaklab.umd.edu/**.

Author contributions

S. M. and H. B. conceived the idea and designed the experiments and simulations for this research. P. L performed the simulations and O. S. performed the experiments. Data analysis were done jointly by S. M., H. B., P. L., O. S. and N. N. The manuscript was written by P. L., H. B. and S. M.

Conflicts of interest

There are no conflicts to declare.

Acknowledgements

We acknowledge financial support from the National Science Foundation (CBET-1760879 for PL and SM and CBET-1800442 for OS and HB) and computational resources at the University of Maryland.

Notes and references

1 H. Weingärtner, C. Cabrele and C. Herrmann, *Phys. Chem. Chem. Phys.*, 2012, **14**, 415–426.
2 H. Zhao, *J. Chem. Technol. Biotechnol.*, 2016, **91**, 25–50.
3 S. K. Shukla and J.-P. Mikkola, *Front. Chem.*, 2020, **8**, 598662.
4 M. Klähn, G. S. Lim and P. Wu, *Phys. Chem. Chem. Phys.*, 2011, **13**, 18647–18660.
5 D. Constantinescu, H. Weingärtner and C. Herrmann, *Angew. Chem., Int. Ed.*, 2007, **46**, 8887–8889.
6 T. Takekiyo, K. Yamazaki, E. Yamaguchi, H. Abe and Y. Yoshimura, *J. Phys. Chem. B*, 2012, **116**, 11092–11097.
7 E. C. Wijaya, F. Separovic, C. J. Drummond and T. L. Greaves, *Phys. Chem. Chem. Phys.*, 2016, **18**, 25926–25936.
8 N. Byrne and C. Angell, *J. Mol. Biol.*, 2008, **378**, 707–714.
9 K. Fujita, D. R. MacFarlane and M. Forsyth, *Chem. Commun.*, 2005, 4804–4806.
10 S. N. Baker, H. Zhao, S. Pandey, W. T. Heller, F. V. Bright and G. A. Baker, *Phys. Chem. Chem. Phys.*, 2011, **13**, 3642–3644.

11 I. Jha and P. Venkatesu, *ACS Sustainable Chem. Eng.*, 2016, **4**, 413–421.
12 F. Deive, A. Rodriguez, A. Pereiro, J. Araújo, M. Longo, M. Coelho, J. C. Lopes, J. Esperança, L. Rebelo and I. Marrucho, *Green Chem.*, 2011, **13**, 390–396.
13 Q. Han, X. Wang and N. Byrne, *ChemCatChem*, 2016, **8**, 1551–1556.
14 M. Kumari, J. K. Maurya, M. Tasleem, P. Singh and R. Patel, *J. Photochem. Photobiol., B*, 2014, **138**, 27–35.
15 K. Meena, D. Neeraj, M. Neha, D. Ravins and P. Rajan, *J. Biomol. Struct. Dyn.*, 2017, **35**, 2016–2030.
16 R. Patel, M. U. H. Mir, J. K. Maurya, U. K. Singh, N. Maurya, M. u d Parray, A. B. Khan and A. Ali, *Luminescence*, 2015, **30**, 1233–1241.
17 U. K. Singh, M. Kumari, S. H. Khan, H. B. Bohidar and R. Patel, *ACS Sustainable Chem. Eng.*, 2018, **6**, 803–815.
18 L. Bui-Le, C. Clarke and A. Bröhl, *Commun. Chem.*, 2020, **3**, 55.
19 N. Debeljuh, C. J. Barrow, L. Henderson and N. Byrne, *Chem. Commun.*, 2011, **47**, 6371–6373.
20 N. Debeljuh, C. J. Barrow and N. Byrne, *Phys. Chem. Chem. Phys.*, 2011, **13**, 16534–16536.
21 R. Zhou, *Proc. Natl. Acad. Sci. U. S. A.*, 2003, **100**, 13280–13285.
22 J. Juraszek and P. Bolhuis, *Proc. Natl. Acad. Sci. U. S. A.*, 2006, **103**, 15859–15864.
23 L. Qiu, S. A. Pabit, A. E. Roitberg and S. J. Hagen, *J. Am. Chem. Soc.*, 2002, **124**, 12952–12953.
24 W. W. Streicher and G. I. Makhatadze, *J. Am. Chem. Soc.*, 2006, **128**, 30–31.
25 M. Gupta, P. Khatua, C. Chakravarty and S. Bandyopadhyay, *J. Phys. Chem. B*, 2018, **122**, 1560–1572.
26 J. L. Huang, M. E. Noss, K. M. Schmidt, L. Murray and M. R. Bunagan, *Chem. Commun.*, 2011, **47**, 8007–8009.
27 A. A. Tietze, F. Bordusa, R. Giernoth, D. Imhof, T. Lenzer, A. Maaß, C. Mrestani-Klaus, I. Neundorf, K. Oum, D. Reith and A. Stark, *ChemPhysChem*, 2013, **14**, 4044–4064.
28 B. Uralcan, S. B. Kim, C. E. Markwalter, R. K. Prudhomme and P. G. Debenedetti, *J. Phys. Chem. B*, 2018, **122**, 5707–5715.
29 D. Diddens, V. Lesch, A. Heuer and J. Smiatek, *Phys. Chem. Chem. Phys.*, 2017, **19**, 20430–20440.
30 V. Lesch, A. Heuer, V. A. Tatsis, C. Holm and J. Smiatek, *Phys. Chem. Chem. Phys.*, 2015, **17**, 26049–26053.
31 H. Vahedian-Movahed, M. R. Saberi and J. Chamani, *J. Biomol. Struct. Dyn.*, 2011, **28**, 483–502.
32 A. Sharifi-Rad, J. Mehrzad, M. Darroudi, M. R. Saberi and J. Chamani, *J. Biomol. Struct. Dyn.*, 2021, **39**, 1029–1043.
33 S. Zohreh, I. Hediye, A. Ahmad, S. Mohammad Reza, M. Mahboobeh and C. Jamshidkhan, *Spectrochim. Acta, Part A*, 2012, **97**, 1089–1100.
34 R. Taheri, N. Hamzkanlu, Y. Rezvani, S. Niroumand, F. Samandar, Z. Amiri-Tehranizadeh, M. R. Saberi and J. Chamani, *J. Mol. Liq.*, 2022, **368**, 120826.
35 A. Sahoo, P.-Y. Lee and S. Matysiak, *J. Chem. Theory Comput.*, 2022, **18**, 5046–5055.
36 M. J. Abraham, T. Murtola, R. Schulz, S. Páll, J. C. Smith, B. Hess and E. Lindahl, *SoftwareX*, 2015, **1–2**, 19–25.
37 H. M. Berman, J. Westbrook, Z. Feng, G. Gilliland, T. N. Bhat, H. Weissig, I. N. Shindyalov and P. E. Bourne, *Nucleic Acids Res.*, 2000, **28**, 235–242.
38 J. W. Neidigh, R. M. Fesinmeyer and N. H. Andersen, *Nat. Struct. Biol.*, 2002, **9**, 425–430.
39 A. G. Cochran, N. J. Skelton and M. A. Starovasnik, *Proc. Natl. Acad. Sci. U. S. A.*, 2001, **98**, 5578–5583.
40 L. I. Vazquez-Salazar, M. Selle, A. H. de Vries, S. J. Marrink and P. C. T. Souza, *Green Chem.*, 2020, **22**, 7376–7386.
41 L. I. Vazquez-Salazar, M. Selle, A. H. De Vries, S. J. Marrink and P. C. Souza, *Green Chem.*, 2020, **22**, 7376–7386.
42 S. O. Yesylevskyy, L. V. Schäfer, D. Sengupta and S. J. Marrink, *PLoS Comput. Biol.*, 2010, **6**, e1000810.
43 T. Darden, D. York and L. Pedersen, *J. Chem. Phys.*, 1993, **98**, 10089–10092.
44 H. A. Posch, W. G. Hoover and F. J. Vesely, *Phys. Rev. A: At., Mol., Opt. Phys.*, 1986, **33**, 4253–4265.
45 B. Hess, H. Bekker, H. J. C. Berendsen and J. G. E. M. Fraaije, *J. Comput. Chem.*, 1998, **19**(18), 1463–1472.
46 M. R. Shirts and J. D. Chodera, *J. Chem. Phys.*, 2008, **129**, 124105.
47 W. Humphrey, A. Dalke and K. Schulten, *J. Mol. Graphics*, 1996, **14**, 33–38.
48 J. Kimball, J. Chavez, L. Ceresa, E. Kitchner, Z. Nurekeyev, H. Doan, M. Szabelski, J. Borejdo, I. Gryczynski and Z. Gryczynski, *Methods Appl. Fluoresc.*, 2020, **8**, 033002.
49 S. K. Panigrahi and A. K. Mishra, *J. Photochem. Photobiol., C*, 2019, **41**, 100318.
50 M. P. Marszall, T. Baczek and R. Kaliszan, *J. Sep. Sci.*, 2006, **29**, 1138–1145.
51 Y. Shiraishi, S. Sumiya, Y. Kohno and T. Hirai, *J. Org. Chem.*, 2008, **73**, 8571–8574.
52 B. K. Paul, A. Samanta and N. Guchhait, *J. Phys. Chem. B*, 2010, **114**, 6183–6196.
53 R. B. Martin, *J. Chem. Educ.*, 1997, **74**, 1238–1240.
54 P. Thordarson, *Chem. Soc. Rev.*, 2011, **40**, 1305–1323.
55 J. T. Vivian and P. R. Callis, *Biophys. J.*, 2001, **80**, 2093–2109.
56 A. A. Rodríguez-Sanz, E. M. Cabaleiro-Lago and J. Rodríguez-Otero, *Org. Biomol. Chem.*, 2015, **13**, 7961–7972.
57 O. Singh, P.-Y. Lee, S. Matysiak and H. Bermudez, *Phys. Chem. Chem. Phys.*, 2020, **22**, 19779–19786.
58 P. Attri, P. Venkatesu and A. Kumar, *Phys. Chem. Chem. Phys.*, 2011, **13**, 2788–2796.
59 W. W. Streicher and G. I. Makhatadze, *Biochemistry*, 2007, **46**, 2876–2880.
60 J. M. Scholtz, D. Barrick, E. J. York, J. M. Stewart and R. L. Baldwin, *Proc. Natl. Acad. Sci. U. S. A.*, 1995, **92**, 185–189.
61 J. M. Scholtz, H. Qian, E. J. York, J. M. Stewart and R. L. Baldwin, *Biopolymers*, 1991, **31**, 1463–1470.
62 C. Toniolo, A. Polese, F. Formaggio, M. Crisma and J. Kamphuis, *J. Am. Chem. Soc.*, 1996, **118**, 2744–2745.
63 Ø. Jacobsen, J. Klaveness, O. P. Ottersen, M. R. Amiry-Moghaddam and P. Rongved, *Org. Biomol. Chem.*, 2009, **7**, 1599.
64 M. C. Manning and R. W. Woody, *Biopolymers*, 1991, **31**, 569–586.
65 M. P. Marszall, T. Baczek and R. Kaliszan, *J. Am. Chem. Soc.*, 2003, **125**, 9038–9047.
66 J. A. Vila, D. R. Ripoll and H. A. Scheraga, *Proc. Natl. Acad. Sci. U. S. A.*, 2000, **97**, 13075–13079.